Variable Switching Point Predictive Current Control for Multi-Phase Permanent Magnet Synchronous Drives

Michael Hoerner ⓘD, *Student Member, IEEE*, Sebastian Wendel ⓘD, *Student Member, IEEE*, Armin Dietz, Petros Karamanakos ⓘD, *Senior Member, IEEE*, and Ralph Kennel, *Senior Member, IEEE*

Abstract—Finite control set model predictive control (FCS-MPC) is a promising method for the control of multi-phase machines, due to its capability to directly account for nonlinearities and multiple controlled variables. To overcome the drawback of high current ripples and excitation of harmonic currents in the so-called xy-subsystem, several methods have been proposed in the literature so far. This paper proposes an MPC-based method that achieves high granularity of switching by not only switching at the discrete time steps, but also within the sampling interval. In doing so, the discussed algorithm, referred to as variable switching point current control (VSP²CC), produces low current distortions, while still keeping the advantages of conventional FCS-MPC, such as fast dynamic behavior during transients. To highlight the above, VSP²CC is applied to a six-phase permanent magnet synchronous machine (PMSM) and compared with conventional FCS-MPC and MPC that employs virtual voltage vectors (VV-MPC).

Index Terms—Model predictive control, FCS-MPC, VSP²CC, VV-MPC, multi-phase, PMSM

I. INTRODUCTION

Due to their capability of fault-tolerance and power segmentation, multi-phase machines got increasing attention by researchers and industry over the last years [1], [2]. Thanks to such advantages as well as their high reliability, multi-phase machines can be used in applications like autonomous driving, more-electric aircrafts and decentralized energy supply [3].

A characteristic property of these machines is the occurrence of low-order current harmonics, due to the low-impedance coupling of the winding subsets. These harmonics can be excited by the geometric properties of the machine as well as by the inverter and can easily lead to a significant total harmonic distortion (THD) in the current. Therefore, one of the main goals of control approaches for multi-phase machines is to avoid excitation of the xy-currents, while maximizing the torque generated by the $\alpha\beta$- or dq-current components.

A control strategy that can be employed to address the above issues is model predictive control (MPC) since it can

M. Hoerner, S. Wendel and A. Dietz are with the Institute for Power Electronic Systems (ELSYS), Nuremberg Institute of Technology, 90489 Nuremberg, Germany; e-mail: michael.hoerner@th-nuernberg.de, sebastian.wendel@th-nuernberg.de, armin.dietz@th-nuernberg.de

P. Karamanakos is with the Faculty of Information Technology and Communication Sciences, Tampere University, 33101 Tampere, Finland; e-mail: p.karamanakos@ieee.org

R. Kennel is with the Chair of Electrical Drive Systems and Power Electronics, Technical University Munich, 80333 Munich, Germany; e-mail: kennel@ieee.org

simultaneously deal with multiple controlled variables (such as the aforementioned current components) in a systematic manner by introducing a cost function that captures all relevant control objectives [4]. Two MPC-based methods that have been applied to multi-phase machines is conventional direct MPC with reference tracking (known also as finite control set MPC—FCS-MPC), and MPC with virtual voltage vectors (VV-MPC) [5]. The former, to achieve good steady-state performance with low current THD requires high granularity of switching, i.e., a high ratio of sampling-to-switching frequency [6]. The latter, aims for a zero average volt-second area in the xy-subsystem over one sampling interval. Though it performs reasonably well in suppressing harmonic currents, it is an open loop concept which always has to apply two active vectors. To overcome this drawback several extensions have been proposed in [7].

An alternative is to use a direct MPC strategy that allows to switch at any time instant within the sampling interval besides the discrete time steps. This method, named variable switching point predictive current control (VSP²CC), was applied to three-phase machines and managed to reduce the stator current distortions owing to the higher granularity of switching [8]. Moreover, thanks to its direct control principle and the possibility to apply only one (instead of two) switch position during transients that results in as short a settling time as possible, both favorable steady-state and dynamic behavior are achieved. Motivated by these, this paper presents a VSP²CC method for multi-phase permanent magnet syn-
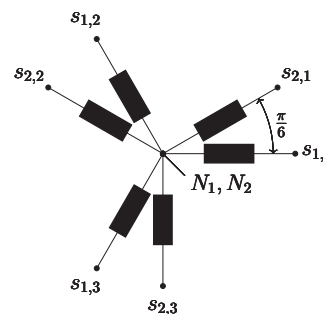

Fig. 1. Six-phase PMSM with phase shift of $\pi/6$ rad between the two subsets of three-phase windings and floating neutral points.

chronous machines (PMSMs). The presented results highlight the superior performance of the drive system as compared with conventional FCS-MPC and VV-MPC.

II. Control Model

The VSP²CC approach is applied to a six-phase PMSM with buried magnets (Fig. 1) which is supplied by a six-phase two-level voltage source inverter (VSI), shown in Fig. 2. The PMSM contains two subsets of three-phase windings with an electrical phase shift of $\pi/6$ between them. The vector space decomposition (VSD) transformation [9], [10], is used to transform the natural phase quantities into the $\alpha\beta$-, xy-, and 0-subspace. Due to the floating neutral points, N_1 and N_2 in Fig. 1, the 0-component is neglected. Further, the $\alpha\beta$-currents are transformed to the rotor-fixed dq-domain by applying the Park transformation.

A. Model Transformations

The VSD transformation matrix $\boldsymbol{T}_{\text{VSD}}$ is given by

$$\boldsymbol{T}_{\text{VSD}} = \frac{1}{3} \begin{bmatrix} 1 & -\frac{1}{2} & -\frac{1}{2} & \frac{\sqrt{3}}{2} & -\frac{\sqrt{3}}{2} & 0 \\ 0 & \frac{\sqrt{3}}{2} & -\frac{\sqrt{3}}{2} & \frac{1}{2} & \frac{1}{2} & -1 \\ 1 & -\frac{1}{2} & -\frac{1}{2} & -\frac{\sqrt{3}}{2} & \frac{\sqrt{3}}{2} & 0 \\ 0 & -\frac{\sqrt{3}}{2} & \frac{\sqrt{3}}{2} & \frac{1}{2} & \frac{1}{2} & -1 \\ 1 & 1 & 1 & 0 & 0 & 0 \\ 0 & 0 & 0 & 1 & 1 & 1 \end{bmatrix} \quad (1)$$

and is applied to the stator currents as shown below

$$\boldsymbol{i}_{\text{vsd}} = \boldsymbol{T}_{\text{VSD}} \boldsymbol{i}_{\text{s}} \quad (2)$$

where the stator current vector is $\boldsymbol{i}_{\text{s}} = [i_{a1}\ i_{b1}\ i_{c1}\ i_{a2}\ i_{b2}\ i_{c2}]^T$ and $\boldsymbol{i}_{\text{vsd}} = [i_\alpha\ i_\beta\ i_x\ i_y\ i_0^+\ i_0^-]^T$ is the VSD transformed current vector. The $\alpha\beta$-currents are transformed to the rotor-fixed dq-frame using

$$\begin{bmatrix} i_d \\ i_q \end{bmatrix} = \begin{bmatrix} \cos(\varphi_{el}) & \sin(\varphi_{el}) \\ -\sin(\varphi_{el}) & \cos(\varphi_{el}) \end{bmatrix} \begin{bmatrix} i_\alpha \\ i_\beta \end{bmatrix} \quad (3)$$

where φ_{el} is the electrical angular position of the rotor giving $\boldsymbol{i}_{\text{VSD}} = [i_d\ i_q\ i_x\ i_y]^T$. The i_0^+ and i_0^- current components are neglected, due to the Y-connected loads with floating neutral points.

B. Prediction Model

The forward-Euler-discretized prediction model of the six-phase PMSM in the dq-, xy-frame can be written as

$$i_d(k+1) = \frac{T_s}{L_d}(v_d(k) - i_d(k)R_s + \omega_{el}(k)L_q i_q(k) + i_d(k) \quad (4a)$$

$$i_q(k+1) = \frac{T_s}{L_q}[v_q(k) - i_q(k)R_s - \omega_{el}(k)(\psi_{\text{pm}} \\ + i_d(k)L_d)] + i_q(k) \quad (4b)$$

$$i_x(k+1) = \frac{T_s}{L_x}(v_x(k) - i_x(k)R_s) + i_x(k) \quad (4c)$$

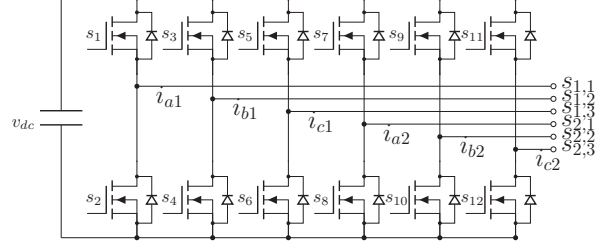$$i_y(k+1) = \frac{T_s}{L_y}(v_y(k) - i_y(k)R_s) + i_y(k) \quad (4d)$$

Fig. 2. Six-phase two-level voltage source inverter.

where T_s is the sampling interval, v_d, v_q, v_x and v_y the voltages in the respective axis, L_d, L_q, L_x and L_y the absolute inductances, R_s the ohmic resistance of one stator phase, ω_{el} the electrical angular frequency, and ψ_{pm} the flux linkage of the permanent magnets.

C. Applicable Voltage Vectors

The $2^6 = 64$ possible switch positions of the VSI and their respective phase voltages applied to the windings of the PMSM are also transformed using the VSD matrix (1) and are shown in Fig. 3. For the sake of convenience, the voltage vectors are drawn as points and have to be thought as space vectors starting from the origin. They are numbered according to the convention that the binary pattern of the vector of the single-phase switch positions in Fig. 2 $\boldsymbol{u}(n) = [s_{11}\ s_9\ s_7\ s_5\ s_3\ s_1]^T$ with $n \in \{0, \ldots, 63\}$ is casted to its respective integer (e.g., $\boldsymbol{u}(27) = [0\ 1\ 1\ 0\ 1\ 1]^T$). The transformed voltage components v_d, v_q, v_x and v_y are used as input variables to the prediction model (4).

III. Variable Switching Point Predictive Current Control For Multi-Phase Machines

The key feature of VSP²CC is the possibility of inserting a variable switching time instant within the sampling interval, as shown in Fig. 4. The algorithm decides whether a single (active or zero) voltage space vector (SV), or a combination of two SVs (two active SVs, or one active SV combined with a zero SV) is applied at the next sampling interval, in order to achieve the regulation of the transformed dq- and xy-currents along their reference values in the best possible way. This method preserves the dynamics of the conventional FCS-MPC, but opens up the possibility of reducing the current ripple by means of refined granularity of the switching instants. Especially the latter point can be advantageous in the control of the xy-currents.

A. Pre-selection Based on the Deadbeat Control Action

In order to reduce the computational burden, the 64 possible switch positions of the VSI are reduced in a heuristic manner. Pre-selection is done by dividing the voltage vectors of the $\alpha\beta$-subspace into 12 sectors, indicated by the roman numbers in Fig. 3. For the VV-MPC always a large SV and the next smaller SV are combined to form a virtual voltage vector inside one sector [5], e.g., 11 and 25 in Sector II. In order to compare VSP²CC with VV-MPC, the active switch positions
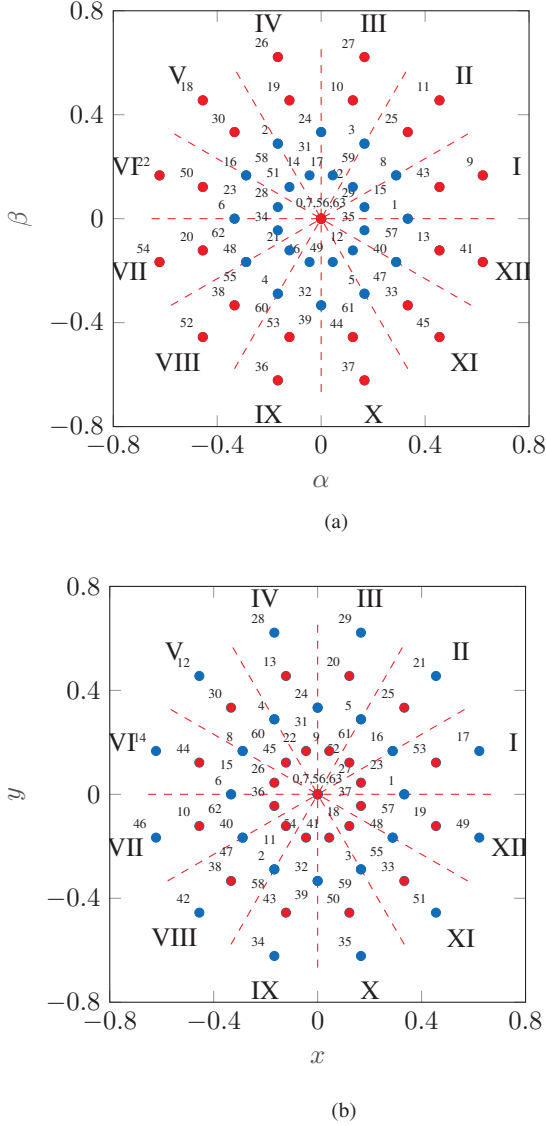
(a)

(b)

Fig. 3. Per unit voltage vectors (a) in the $\alpha\beta$- and (b) xy-plane .

from which to choose are limited to the same options as with the VV-MPC, but with the freedom to additionally choose from zero SVs, e.g., in Sector II vectors $0, 11, 25$ and 63 are respected, indicated by the red dots. For determination of the correct sector and for further reduction of the candidate switch positions, a heuristic pre-selection according to the deadbeat control action is conducted in the dq-domain. Specifically, according to the following equations

$$v_d^*(k) = L_d \frac{i_d^*(k) - i_d(k)}{T_s} + R_s i_d(k) - \omega_m(k)pL_q i_q(k) \tag{5a}$$

$$v_q^*(k) = L_q \frac{i_q^*(k) - i_q(k)}{T_s} + R_s i_q(k) + \omega_m(k)pL_d i_d(k) + \omega_m(k)p\psi_{\text{pm}} \tag{5b}$$

the deadbeat solution, i.e., the desired voltage that drives the dq-currents to their references at the end of one sampling

interval T_s is computed. Limitations of the available voltage are of no concern at this point; only the resulting angle

$$\gamma(k) = \arctan 2(v_q^*(k), v_d^*(k)) + \varphi_{el}, \{\gamma \in \mathbb{R} | 0 \leq \gamma \leq 2\pi\} \tag{6}$$

is of interest in order to determine the sector formed by the SVs that are to be evaluated by the predictive algorithm. The resulting angle $\gamma(k)$ is mapped to the respective SVs and sector according to the subsequent case distinction

$$\boldsymbol{SV}(k) = \begin{cases} 0, 9, 43, 63 & \text{if } 0 \leq \gamma(k) \leq \frac{\pi}{6} & \text{(I)} \\ 0, 11, 25, 63 & \text{if } \frac{\pi}{6} < \gamma(k) \leq \frac{\pi}{3} & \text{(II)} \\ 0, 10, 27, 63 & \text{if } \frac{\pi}{3} < \gamma(k) \leq \frac{\pi}{2} & \text{(III)} \\ 0, 19, 26, 63 & \text{if } \frac{\pi}{2} < \gamma(k) \leq \frac{2\pi}{3} & \text{(IV)} \\ 0, 18, 30, 63 & \text{if } \frac{2\pi}{3} < \gamma(k) \leq \frac{5\pi}{6} & \text{(V)} \\ 0, 22, 50, 63 & \text{if } \frac{5\pi}{6} < \gamma(k) \leq \pi & \text{(VI)} \\ 0, 20, 54, 63 & \text{if } \pi < \gamma(k) \leq \frac{7\pi}{6} & \text{(VII)} \\ 0, 38, 52, 63 & \text{if } \frac{7\pi}{6} < \gamma(k) \leq \frac{4\pi}{3} & \text{(VIII)} \\ 0, 36, 53, 63 & \text{if } \frac{4\pi}{3} < \gamma(k) \leq \frac{3\pi}{2} & \text{(IX)} \\ 0, 37, 44, 63 & \text{if } \frac{3\pi}{2} < \gamma(k) \leq \frac{5\pi}{3} & \text{(X)} \\ 0, 33, 45, 63 & \text{if } \frac{5\pi}{3} < \gamma(k) \leq \frac{11\pi}{6} & \text{(XI)} \\ 0, 13, 41, 63 & \text{if } \frac{11\pi}{6} < \gamma(k) \leq 2\pi & \text{(XII)} \end{cases}$$

For the considerations of the VSP²CC algorithm it is not necessary to decide which zero vector will be evaluated at this point. Specifically, if a zero SV is chosen by VSP²CC, then the algorithm has the ability to choose that one that results in the minimum number of switching transitions, as implied by the formulated cost function in Section III-C.

B. Current Slopes and Variable Switching Point

The VSP²CC approach is based on the assumption that the sampling frequency is high enough so that the evolution of the current slopes within one sampling interval can be thought linear, as shown in the example of the current i_d in Fig. 4. Other nonlinearities, such as saturation and cross-coupling, or slowly time-varying parameter shifts are neglected within the sampling interval T_s. Therefore, the slope of each current component can be calculated by

$$\boldsymbol{m}(k) = \frac{\boldsymbol{i}_{\text{vsd}}(k+1) - \boldsymbol{i}_{\text{vsd}}(k)}{T_s} = \frac{\Delta \boldsymbol{i}_{\text{vsd}}}{T_s}, \tag{7}$$

where $\boldsymbol{m}(k) = [m_d(k)\ m_q(k)\ m_x(k)\ m_y(k)]^T$. This way it is possible to compensate for the delay of one sampling interval and calculate the currents at time step $k+1$ ($i_{d,\text{delay}}$ in Fig. 4).

Moreover, the evolution of the currents within the prediction horizon can be computed. Starting at time step k it can be seen that with respect to the applied voltage vectors, selected in the previous sampling period (in this example a variable switching point $t_z(k)$ is inserted), the slopes of the currents and their evolution are calculated. Therefore, the currents $\boldsymbol{i}_{\text{vsd}}(k+1)$ at time step $k + 1$ can be computed. Taking into account the reduced set of voltage vectors in the considered sector, currents may evolve with three different slopes, depending
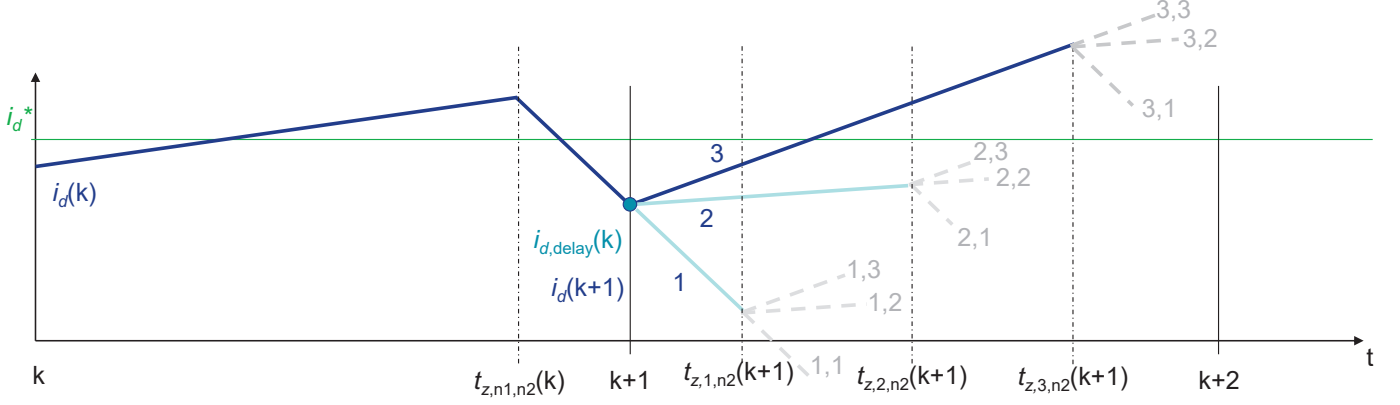
Fig. 4. Current slopes and variable switching points a the example of the i_d-current.

on the voltage vector. Due to the possibility of inserting a variable switching point, each of the three current slopes (1 to 3 in Fig. 4) can be combined with one of the other two slopes at any time instant within the sampling interval. This means that a single SV will be applied for the whole sampling interval T_s so that the current evolves with one constant slope, or two different voltage vectors are applied within T_s (one at the beginning of T_s and the other at the variable switching point t_z) such that the current within T_s will evolve with two different slopes. This way, nine different cases have to be evaluated from the MPC algorithm. In Fig. 4 this is shown at the example of the current i_d, but the same principle applies to i_q, i_x, and i_y. Each combination of slopes will lead to a specific deviation from the reference current, while the switching instant still remains as a variable.

The difference between the piecewise linear currents and their reference values are integrated and summed up, in order to calculate the rms error $e_{\text{rms}^2 n1,n2}$ of all current components over the present prediction period

$$
\begin{aligned}
e_{\text{rms}^2 n1,n2}(t_z) = \frac{1}{T_s} \bigg(& \int_0^{t_{z,n1,n2}} (i_{d,0} + m_{d,n1}t - i_d^*)^2 \, \mathrm{d}t \\
& + \int_{t_{z,n1,n2}}^{T_s} (i_{d,t_z} + m_{d,n2}t - i_d^*)^2 \, \mathrm{d}t \\
& + \int_0^{t_{z,n1,n2}} (i_{q,0} + m_{q,n1}t - i_q^*)^2 \, \mathrm{d}t \\
& + \int_{t_{z,n1,n2}}^{T_s} (i_{q,t_z} + m_{q,n2}t - i_q^*)^2 \, \mathrm{d}t \\
& + \int_0^{t_{z,n1,n2}} (i_{x,0} + m_{x,n1}t - i_x^*)^2 \, \mathrm{d}t \\
& + \int_{t_{z,n1,n2}}^{T_s} (i_{x,t_z} + m_{x,n2}t - i_x^*)^2 \, \mathrm{d}t \\
& + \int_0^{t_{z,n1,n2}} (i_{y,0} + m_{y,n1}t - i_y^*)^2 \, \mathrm{d}t \\
& + \int_{t_{z,n1,n2}}^{T_s} (i_{y,t_z} + m_{y,n2}t - i_y^*)^2 \, \mathrm{d}t \bigg), \quad (8)
\end{aligned}
$$

i.e., here, $n1$ and $n2 \in \{1, 2, 3\}$ refer to the first and second part of the slope within one step of the prediction horizon. Setting the derivative of (8) to zero, $\mathrm{d}e_{\text{rms}^2}/\mathrm{d}t_z = 0$ and solving for t_z gives

$$
t_{z,n1,n2} = \frac{a_{n1,n2} + b_{n1,n2} + c_{n1,n2} + d_{n1,n2}}{e_{n1,n2} + f_{n1,n2} + g_{n1,n2} + h_{n1,n2}}, \quad (9)
$$

where

$$
\begin{aligned}
a_{n1,n2} &= (m_{d,n2} - m_{d,n1})(2i_d - 2i_d^* + T_s m_{d,n2}), \\
b_{n1,n2} &= (m_{q,n2} - m_{q,n1})(2i_q - 2i_q^* + T_s m_{q,n2}), \\
c_{n1,n2} &= (m_{x,n2} - m_{x,n1})(2i_x - 2i_x^* + T_s m_{x,n2}), \\
d_{n1,n2} &= (m_{y,n2} - m_{y,n1})(2i_y - 2i_y^* + T_s m_{x,n2}), \\
e_{n1,n2} &= (m_{d,n1} - m_{d,n2})(2m_{d,n1} - m_{d,n2}), \\
f_{n1,n2} &= (m_{q,n1} - m_{q,n2})(2m_{q,n1} - m_{q,n2}), \\
g_{n1,n2} &= (m_{x,n1} - m_{x,n2})(2m_{x,n1} - m_{x,n2}), \\
h_{n1,n2} &= (m_{y,n1} - m_{y,n2})(2m_{y,n1} - m_{y,n2}).
\end{aligned}
$$

As can be understood, with (9) in total 9 switching times $t_{z,n1,n2}$ are calculated in total, where all combinations of the considered voltage vectors and their respective current gradients are evaluated. For each of them, the resulting $t_{z,n1,n2}$ minimizes $e_{\text{rms}^2 n1,n2}$ for the specific combination. However, not all of them might fulfill the condition $0 \leq t_{z,n1,n2} \leq T_s$. Switching times that are not within the sampling interval automatically lead to single vectors, which are implemented for the whole interval. The same principle also applies to the cases where $n1 = n2$.

C. Cost Function

All computed switching times $t_{z,n1,n2}$ are further evaluated with their corresponding currents and the currents at the end of each sampling interval in the cost function. In addition, current limits are imposed for safety reasons, and the switching effort
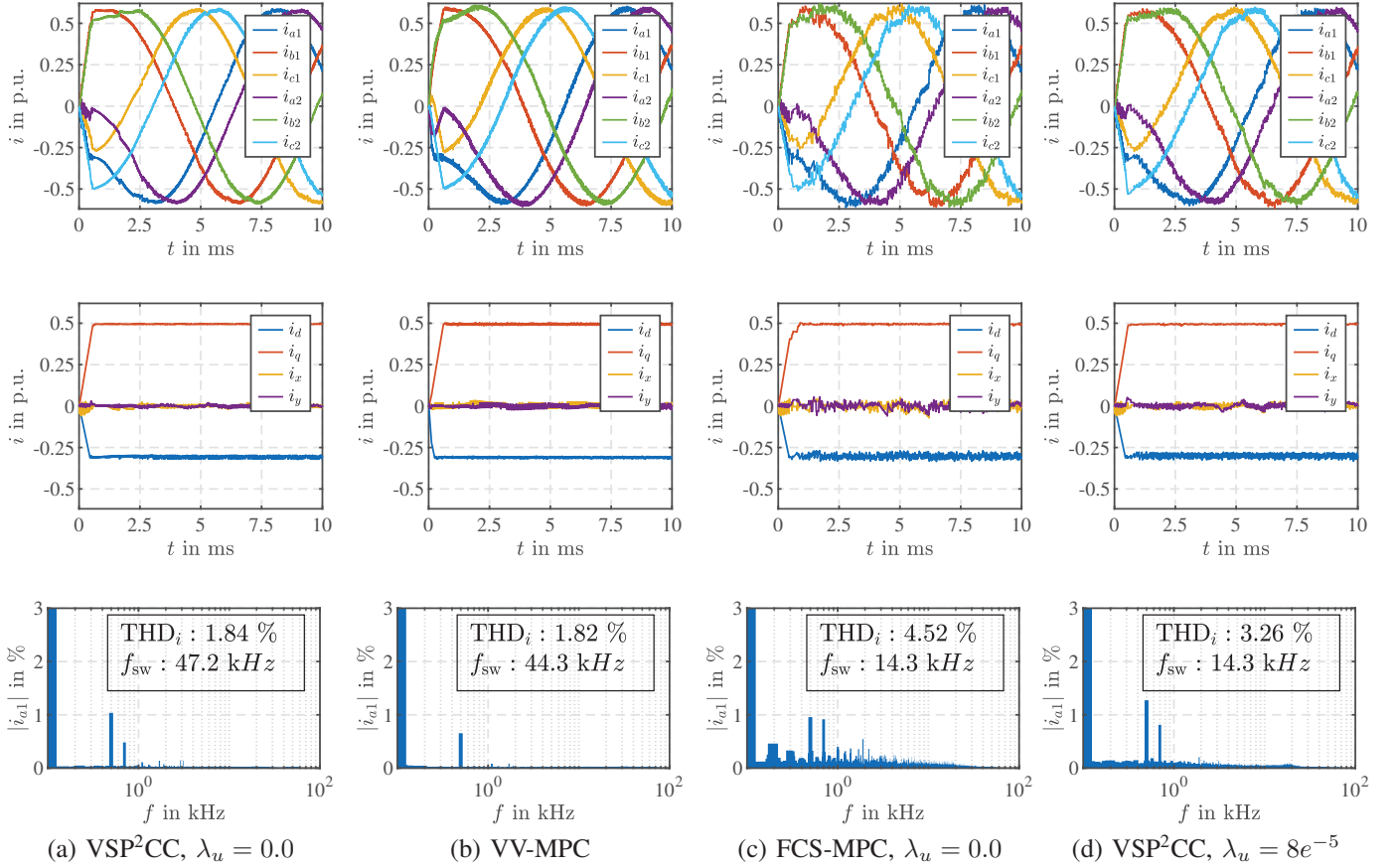
Fig. 5. First row: phase currents, second row: $\boldsymbol{i}_{\mathrm{vsd}}$ and third row: THD_i of the current i_{a1}. (a) $\mathrm{VSP^2CC}$, (b) VV-MPC, (c) FCS-MPC and (d) $\mathrm{VSP^2CC}$ with $\lambda_u = 8e^{-5}$. Operating point (p.u.): $n = 0.5$, $i_d^* = -0.31$, $i_q^* = 0.5$, $i_x^* = 0.0$, $i_y^* = 0.0$, $f_s = 1/T_s = 100$ kHz. All THD_i are averaged from all six phase currents over 20 fundamental periods.

is penalized to reduce the switching frequency, and thus the power losses. This leads to the cost function

$$
\begin{aligned}
J(k) = \sum_{\ell=k}^{k+N_p-1} & \bigg(||\boldsymbol{i}_{\mathrm{vsd},t_z}(\ell+1) - \boldsymbol{i}_{\mathrm{vsd}}^*(k)||_2^2 \\
& + ||\boldsymbol{i}_{\mathrm{vsd},T_s}(\ell+1) - \boldsymbol{i}_{\mathrm{vsd}}^*(k)||_2^2 \\
& + \hat{f}(\boldsymbol{i}_{\mathrm{vsd}}(\ell+1)) + \lambda_u ||\Delta\boldsymbol{u}(\ell)||_1 \bigg) \quad (10)
\end{aligned}
$$

with $\hat{f}(\boldsymbol{i}_{\mathrm{vsd}}(\ell+1)) = \begin{cases} 4 & \text{if } ||\boldsymbol{i}_{\mathrm{vsd}}(\ell+1)||_2 > i_{\max} \\ 0 & \text{if } ||\boldsymbol{i}_{\mathrm{vsd}}(\ell+1)||_2 \le i_{\max} \end{cases}$

where N_p is the prediction horizon (here chosen as $N_p = 1$), $\hat{f}$ is a hard constraint taking into account the maximum allowed current $i_{\max}$,[1] where "4" is the maximum current in per unit (p.u.), λ_u is a nonnegative weighting factor for controlling the average switching frequency and $\Delta\boldsymbol{u}$ the difference between two consecutive switch positions, as described in [6]. All current components inside the cost function (10) are equally weighted for all subsequent considerations.

[1] In general a soft constraint is to be preferred since it can avoid feasibility problems when solving (10).

IV. SIMULATION RESULTS

The presented $\mathrm{VSP^2CC}$ is evaluated in simulation on the example of a six-phase PMSM, using the parameters shown in Table I and taken from [11]. The implementation is done in the p.u. system and all parameters and values are transformed according to [12, Ch. 2.1.2]. The simulation results are compared with VV-MPC taken from [5] and conventional FCS-MPC. The simulation starts with constant speed of the motor $n = 0.5$ followed by a load step from $\boldsymbol{i}_{\mathrm{vsd}}^* = \boldsymbol{0}$ to $i_d^* = -0.31$ p.u. and $i_q^* = 0.5$ p.u.

A. Steady-State Performance

Fig. 5 shows the comparison of the different control approaches at specific operating point. Column (a) is the $\mathrm{VSP^2CC}$ approach without penalization of the switching effort ($\lambda_u = 0$) which is compared at an almost equal average switching frequency with the VV-MPC approach in column (b). In (c) the conventional FCS-MPC is shown, using the heuristic pre-selection described in section III-A and without penalization of the switching. Column (d) again shows the $\mathrm{VSP^2CC}$ approach but with $\lambda_u = 8e^{-5}$ in order to achieve the same average switching frequency as FCS-MPC. Considering (a) and (b), $\mathrm{VSP^2CC}$ shows comparable performance to the
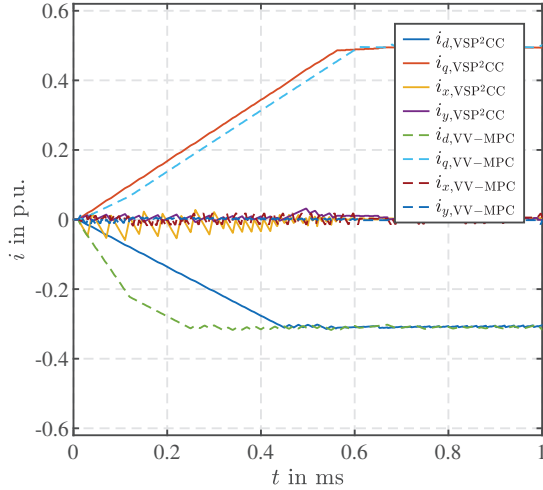
Fig. 6. Comparison of the dynamic behavior of (a) and (b) from Fig. 5.

TABLE I
SIMULATION PARAMETERS

Parameter	Symbol	Value	Unit
winding resistance	R_s	0.035	Ohm
d-axis inductance	L_d	0.82	mH
q-axis inductance	L_q	2.49	mH
x- and y-axis inductance	L_x, L_y	0.27	mH
PM flux linkage	ψ_{pm}	0.034	Vs
pole pairs	p	3	1
dc-link voltage	v_{dc}	270	V
Sampling frequency	f_s	100	kHz
mechanical rotor speed	n	0.5	p.u.
d-axis reference current	i_d^*	-0.31	p.u.
q-axis reference current	i_q^*	0.5	p.u.
x-axis reference current	i_x^*	0.0	p.u.
y-axis reference current	i_y^*	0.0	p.u.

VV-MPC with respect to the THD_i. Both achieve almost zero currents in the xy-subspace. In (c) and (d) FCS-MPC is compared to VSP^{2}CC at an equal average switching frequency by introducing penalization of the switching effort to the VSP^{2}CC. As expected, FCS-MPC leads to the largest THD_i with insufficient control of the harmonic xy-currents, due to the lack of switching granularity. On the other hand, VSP^{2}CC results in improvement of the THD_i of 1.26 %.

B. Dynamic Performance

Fig. 6 shows the dynamic response to the load step ($\boldsymbol{i}_{\mathrm{vsd}}^* = \boldsymbol{0}$ to $\boldsymbol{i}_{\mathrm{vsd}}^* = [-0.31\ 0.5\ 0\ 0]^T$) at the beginning of the simulation of VSP^{2}CC and VV-MPC. Due to its ability to apply only one active SV during transients, VSP^{2}CC manages to have an as short settling time as possible. As can be seen, VV-MPC manages to regulate the d-current slightly faster than VSP^{2}CC owing to its ability to control only the dq-currents, while the xy-currents are merely indirectly controlled. However, to achieve this, VV-MPC switches at much higher frequency than VSP^{2}CC, implying that the generated power losses are also higher.

V. CONCLUSION

The presented VSP^{2}CC approach shows superior performance over conventional FCS-MPC in steady-state and comparable performance to VV-MPC with respect to the THD_i. The methodology is presented at the example of a six-phase PMSM but can be easily extended to higher phase numbers, where additional harmonic subsystems have to be accounted for in the calculation of the variable switching point t_z. During transients VSP^{2}CC responds faster than VV-MPC, due to the freedom of applying active voltage vectors for the whole sampling interval. This, however, occurs at the cost of less control of the xy-currents, which is no disadvantage during usual short transients.

In the future, further examination will be done on different finite control sets with more or different pre-selected voltage vectors. Moreover, the discussed VSP^{2}CC concept will be extended to higher phase numbers. Finally, the efficacy of the proposed control scheme will be experimentally verified.

REFERENCES

[1] A. Salem and M. Narimani, "A review on multiphase drives for automotive traction applications," *IEEE Trans. Transport. Electrif.*, vol. 5, no. 4, pp. 1329–1348, 2019.
[2] P. F. C. Gonçalves, S. M. A. Cruz, and A. M. S. Mendes, "Predictive current control of six-phase permanent magnet synchronous machines based on virtual vectors with optimal amplitude and phase," in *Int. Conf. Smart Energ. Syst. Technol.*, 2019, pp. 1–6.
[3] E. Levi, "Multiphase electric machines for variable-speed applications," *IEEE Trans. Ind. Electron.*, vol. 55, no. 5, pp. 1893–1909, 2008.
[4] P. Karamanakos, E. Liegmann, T. Geyer, and R. Kennel, "Model predictive control of power electronic systems: Methods, results, and challenges," *IEEE Open J. Ind. Appl.*, vol. 1, pp. 95–114, 2020.
[5] I. Gonzalez-Prieto, M. J. Duran, J. J. Aciego, C. Martin, and F. Barrero, "Model predictive control of six-phase induction motor drives using virtual voltage vectors," *IEEE Trans. Ind. Electron.*, vol. 65, no. 1, pp. 27–37, 2018.
[6] P. Karamanakos and T. Geyer, "Guidelines for the design of finite control set model predictive controllers," *IEEE Trans. Power Electron.*, vol. 35, no. 7, pp. 7434–7450, Jul. 2020.
[7] A. González-Prieto, I. González-Prieto, and M. J. Duran, "Smart voltage vectors for model predictive control of six-phase electric drives," *IEEE Trans. Ind. Electron.*, vol. 68, no. 10, pp. 9024–9035, 2021.
[8] S. Wendel, P. Karamanakos, A. Dietz, and R. Kennel, "Operating point dependent variable switching point predictive current control for PMSM drives," in *Proc. IEEE Int. Symp. Pred. Control of Elect. Drives and Power Electron.*, Quanzhou, China, May/Jun. 2019, pp. 1–6.
[9] Y. Zhao and T. Lipo, "Space vector pwm control of dual three-phase induction machine using vector space decomposition," *IEEE Trans. Ind. Appl.*, vol. 31, no. 5, pp. 1100–1109, 1995.
[10] A. A. Rockhill and T. A. Lipo, "A generalized transformation methodology for polyphase electric machines and networks," in *Proc. IEEE Int. Elect. Mach. Drives Conf.*, 2015, pp. 27–34.
[11] D. Ye, J. Li, R. Qu, H. Lu, and Y. Lu, "Finite set model predictive mtpa control with vsd method for asymmetric six-phase pmsm," in *Proc. IEEE Int. Elect. Mach. Drives Conf.*, 2017, pp. 1–7.
[12] T. Geyer, *Model predictive control of high power converters and industrial drives*. Hoboken, NJ, USA: Wiley, 2016.